We are IntechOpen,
the world's leading publisher of
Open Access books
Built by scientists, for scientists

6,900
Open access books available

186,000
International authors and editors

200M
Downloads

Our authors are among the

154
Countries delivered to

TOP 1%
most cited scientists

12.2%
Contributors from top 500 universities

BOOK CITATION INDEX
CLARIVATE ANALYTICS
INDEXED

WEB OF SCIENCE™

Selection of our books indexed in the Book Citation Index
in Web of Science™ Core Collection (BKCI)

Interested in publishing with us?
Contact book.department@intechopen.com

Numbers displayed above are based on latest data collected.
For more information visit www.intechopen.com

Numerical Analysis of Planar Periodic Multilayer Structures by Method of Moments

Stanislav Gona
Tomas Bata University in Zlin
Czech Republic

1. Introduction

Numerical analysis of planar periodic multilayer structures is often carried out with the aid the method of moments (MoM). The advantage of the technique against the other, more general methods (like FEM and FDTD) is in faster computation of reflection and transmission properties of a periodic structure. Besides of computation speed, usage of MoM typically results in lower memory requirements when compared to FEM and FDTD. The method of moments can be either formulated in the spatial or spectral domain. For analysis of periodic structures the spectral formulation is more advantageous – a discrete space spectrum (Scott, 1989). Thus, the original integral equations reduce into algebraic ones (that is double summations are being used instead of surface integrals). The disadvantage of the spectral formulation is that double summations arising in MoM formulation are slowly convergent and a high number of Floquet modes is needed for analysis of periodic structures having fine patch details inside the periodic cell or densely stacked structures. Simple spectral domain MoM codes for analysis periodic structures consider uniform mesh of cells and utilize FFT to accelerate the double summations (Cwick & Mittra, 1987; Wan & Encinar, 1995). These simple MoM codes also typically use small domain basis functions (like rooftops (Cwick & Mittra, 1987), or triangular (RWG) basis functions (Kipp & Chan, 1994)). If more general geometry is to be analyzed, then a non-uniform mesh of rectangular or quad shaped cells (Kolundzija, 1998) must be used. From the computational point of view it also highly desirable to consider use of higher order large domain basis functions for representation of surface currents. Then, the conductive currents in patches may be accurately described with a small number of unknown expansion coefficients.

Solution of reflection/transmission properties of a multilayer periodic structure can be performed either directly (Wu, 1995) or by the use of a cascade approach (Mittra et. al, 1988) or (Wan & Encinar, 1995). The cascade approach is suitable for periodic structures which with a large or a medium electrical thickness of individual dielectric layers. When the electrical thickness of a particular dielectric layer becomes too small then a large number of Floquet modes must be used during the cascade process (Wan & Encinar, 1995). In such a case, which is a typical for periodic structures with microscopically thin layers (e.g. carbon fibre composite materials) the direct approach is being used.

The chapter is organized as follows. In section 2, the formulation of MoM in the spectral domain is described. The formulation is based on (Wu, 1995) and in the further text it will be referenced as a direct approach. Section 3 describes approximation of surface currents with small domain rooftops defined over a non-uniform mesh of rectangular cells and use of higher order domain basis functions defined over quadrilaterals. Computation of reflection and transmission coefficients is described in section 4. Numerical examples are given in section 5. These examples fall into two different groups. First group belongs to the area of frequency selective surfaces, where results from our in-house MoM code called FSSMQ are compared with those existing in literature. Second group of examples spans into the area of composite materials, where FSSMQ code is used for prediction of shielding effectiveness of a composite with partially conductive carbon fibres. Finally, concluding remarks are given in section 6.

2. Spectral domain method of moments

In this section, a detail overview of the spectral domain method of moments is given. The formulation and notation being used is based on (Wu, 1995) and (Mittra et al., 1988). The formulation is based in the immitance approach developed originally by (Itoh, 1980) and is slightly different from the notation being used by other authors (Scott, 1989). As a new, when compared to existing papers related to the spectral domain MoM, incorporation of non-uniform mesh rectangular cells and mesh of quadrilateral cells is presented in section 3.

2.1 Multilayer problem – formulation (EFIE)

Let's consider a planar periodic multilayer structure according to Fig. 1. As an example structure with 2 dielectric layers is given. Metal layers are denoted as M_0, M_1 and M_2. The top of the dielectric structure is a placed at position $z = 0$.
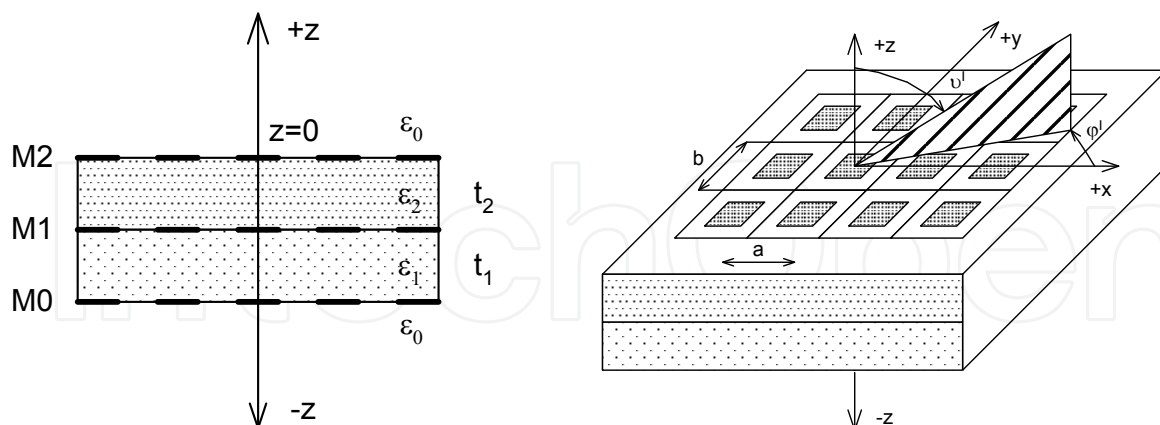

Fig. 1. Left) Multilayer FSS – layer definition, Right) Periodic cell and definition of angles of incidence

The reflection/transmission from the multilayer structure is solved within a single periodic cell dimensioned a and b. The structure is illuminated by the TE or TM polarized plane wave with the angles of incidence ϑ^I and φ^I. The formulation of MoM in the spectral domain starts with expressing an electric intensity of the incident and scattered wave in space and

spectral domain (equations 1 and 2). Then, the electric field integral equation (EFIE), (Scott, 1989) and (Wu, 1995) is formulated in the spectral domain (3).

$$\mathbf{E}_{ii}^{inc}(x,y)e^{j(\alpha_0 x+\beta_0 y)}+\mathbf{E}_{ii}^{scat}(x,y)=Z_s\mathbf{J}_{ii}(x,y) \tag{1}$$

where ii stands for the index of metal layer (ii=0,1,2, …), $\mathbf{E}_{ii}^{inc}(x,y)$ is electric intensity of the incident wave at the ii^{th} metal layer (but with all metal layers removed). The components of intensity $\mathbf{E}_{ii}^{inc}(x,y)$ can be calculated according to a procedure given in section 4. The symbol $\mathbf{E}_{ii}^{scat}(x,y)$ stands for the electric intensity at ii^{th} layer arising from conductive currents from ii^{th} and all remaining metal layers placed above and beneath the ii^{th} metal layer. As metal layers may be lossy, with a finite conductivity σ_{ii} [S/m], then the total tangential electric field is not completely vanishing on the conductors. Such a situation may be approximated with the so called surface impedance Z_s. The surface impedance is determined from the sheet resistance R_s (Cwick & Mittra, 1987) as $Z_s = (1+j)R_s$, where R_s is calculated as $R_S=\sqrt{\omega\mu_{ii}/2\sigma_{ii}}$. The concept of sheet resistance is valid when skin depth is less than the metal thickness. Last two symbols α_0 and β_0 to be explained, stand for x and y components of the wave vector of the incident wave. Time dependence of $e^{j\omega t}$ is assumed in this chapter.

In the subsequent paragraphs, double index ii or jj will used for the index of a metal layer, while the single index i will stand for an integer index of a dielectric layer.

$$\mathbf{E}_{ii}^{inc}(m,n)+\mathbf{E}_{ii}^{scat}(m,n)=Z_s\mathbf{J}_{ii}(m,n) \ \dots \text{ on metal parts of } ii^{th} \text{ metal layer} \tag{2}$$

$$\mathbf{E}_{ii}^{inc}(m,n)+\sum_{jj=0}^{N_m}\begin{bmatrix}G_{xx}^{ii\leftarrow jj} & G_{xy}^{ii\leftarrow jj}\\ G_{yx}^{ii\leftarrow jj} & G_{yy}^{ii\leftarrow jj}\end{bmatrix}\begin{bmatrix}\mathbf{J}_{jj,x}(m,n)\\ \mathbf{J}_{jj,y}(m,n)\end{bmatrix}=Z_s\mathbf{J}_{ii}(m,n) \ ; ii=0,1,...,N_m \tag{3}$$

with $G_{xx}^{ii\leftarrow jj}$, $G_{xy}^{ii\leftarrow jj}$, $G_{yx}^{ii\leftarrow jj}$ and $G_{yy}^{ii\leftarrow jj}$ standing for components of the self and mutual impedance matrix $[G^{ij}]$ which relates the scattered electric field at ii^{th} metal layer through the conductive currents at jj^{th} layer. N_m is index of a maximal metal layer in the analyzed multilayer structure. Symbols m and n have a meaning of integer indexes (Floquet harmonics). These indexes range from $-M$ to $+M$, resp. $-N$ to $+N$, where M, N represent the maximal Floquet harmonics.

$$\mathbf{E}_{ii}=[G^{ij}]\mathbf{J}_{jj} \tag{4}$$

Components of $[G^{ij}]$ are evaluated by the immitance approach (Itoh, 1980) and (Wu, 1995).

The evaluation of $[G^{ij}]$ is different for the case with $ii=jj$ (self-impedance matrix) and $ii\neq jj$ (mutal impedance matrix).

2.2 Self impedance matrixes

In the case of self-impedance matrixes, the total admittance looking up and down from the ii^{th} layer is evaluated in series of steps described below (Wu, 1995). As an example, situation for the two layer dielectric structure is given in Fig . 2.
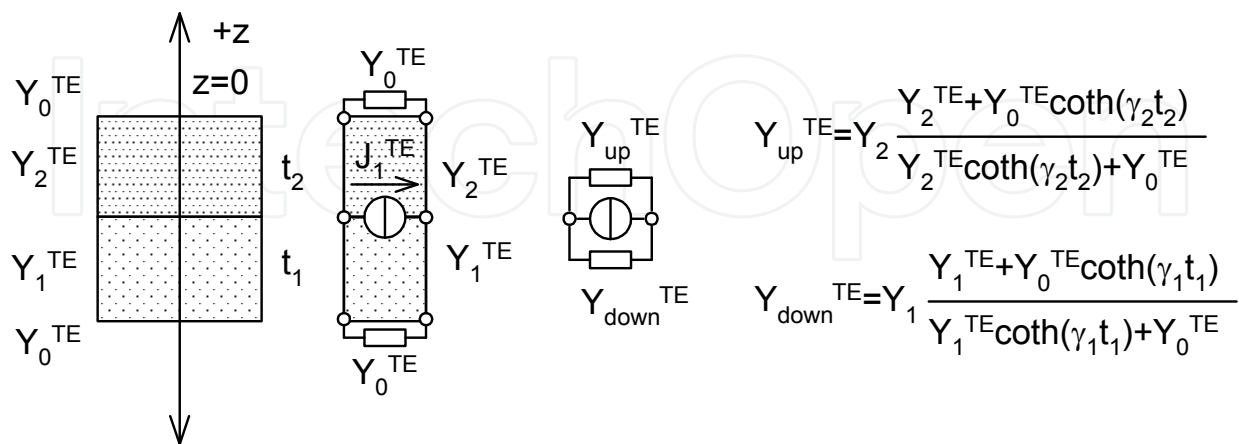

Fig. 2. Multilayer FSS – example of evaluation of up and down looking admittance for the metal layer M1.

Evaluation of up and looking admittance is performed with the aid of the equation (5) known the transmission line theory

$$Y_i^{TE,TM} = Y_i^{TE,TM} \frac{Y_i^{TE,TM} + Y_L \coth(\gamma_i t_i)}{Y_i^{TE,TM} \coth(\gamma_i t_i) + Y_L} \tag{5}$$

where Y_i^{TE} and Y_i^{TM} are TE and TM admittances of the ii^{th} dielectric layer. According to (Wu, 1995) these impedances can be expressed as

$$Y_i^{TE} = \frac{-\gamma_i}{j\omega\mu_i} \tag{6a}$$

$$Y_i^{TM} = \frac{-j\omega\varepsilon_i}{\gamma_i} \tag{6b}$$

Symbol ω stands for the angular frequency, the complex permittivity and permeability of the ii^{th} dielectric layer are denoted as ε_i and μ_i. Last symbol γ_i being used in (6a,b) represents the complex propagation constant in the z-direction (for the ith dielectric layer).

$$\gamma_i = \sqrt{\alpha_m^2 + \beta_n^2 - k_i^2} \tag{7}$$

The propagation constant γ_i is determined upon the transversal propagation constant $k_{xy,i} = \sqrt{\alpha_m^2 + \beta_n^2}$ and the wave number k_i valid for the ith dielectric layer.

Components of the transversal propagation constant $k_{xy,i}$ are called as Floquet harmonics and may be expressed as

$$\alpha_m(m,n) = \alpha_0 + \frac{2\pi}{a}m \tag{8a}$$

$$\beta_n(m,n) = \beta_0 + \frac{2\pi}{b}n \tag{8b}$$

Wave numbers α_0 and β_0 are the fundamental (zeroth order) spectral harmonics and they are directly linked with the incident angles ϑ^I and φ^I by equations (9a) and (9b)

$$\alpha_0 = k_0 \sin(\vartheta^I)\cos(\varphi^I) \tag{9a}$$

$$\beta_0 = k_0 \sin(\vartheta^I)\sin(\varphi^I) \tag{9b}$$

where $k_0 = 2\pi f \sqrt{\mu_0 \varepsilon_0}$ and $k_i = 2\pi f \sqrt{\mu_i \varepsilon_i}$

The total TE and TM impedances connected to the ii^{th} metal layer are then

$$Z_{g,ii}^{TE} = \frac{1}{Y_{down,ii}^{TE} + Y_{up,ii}^{TE}} \tag{10a}$$

$$Z_{g,ii}^{TM} = \frac{1}{Y_{down,ii}^{TM} + Y_{up,ii}^{TM}} \tag{10b}$$

Finally, components of $[G^{ii}]$ can be written (Wu, 1995) as

$$[G^{ii}] = \begin{bmatrix} G_{xx,ii} & G_{xy,ii} \\ G_{yx,ii} & G_{yy,ii} \end{bmatrix} \tag{11}$$

$$G_{xx,ii} = Z_{g,ii}^{TE}\sin^2\Theta + Z_{g,ii}^{TM}\cos^2\Theta \tag{12a}$$

$$G_{xy,ii} = (Z_{g,ii}^{TM} - Z_{g,ii}^{TE})\sin\Theta\cos\Theta \tag{12b}$$

$$G_{yx,ii} = G_{xy,ii} \tag{12c}$$

$$G_{yy,ii} = Z_{g,ii}^{TE}\cos^2\Theta + Z_{g,ii}^{TM}\sin^2\Theta \tag{12d}$$

where

$$\sin\Theta = \frac{\beta}{\sqrt{\alpha^2 + \beta^2}} \tag{13a}$$

$$\cos\Theta = \frac{\alpha}{\sqrt{\alpha^2 + \beta^2}} \tag{13b}$$

2.3 Mutual impedance matrixes

Mutual impedance matrixes $[G^{ij}]$ are evaluated with the aid of self impedance matrix for the ii^{th} layer and the transfer impedance Z_t (Wu, 1995).

$$[G^{ij}] = \begin{bmatrix} G_{xx,ij} & G_{xy,ij} \\ G_{yx,ij} & G_{yy,ij} \end{bmatrix} \tag{14}$$

$$G_{xx,ij} = Z_{g,ij}^{TE} \sin^2\Theta + Z_{g,ij}^{TM} \cos^2\Theta \tag{15a}$$

$$G_{xy,ij} = (Z_{g,ij}^{TM} - Z_{g,ij}^{TE}) \sin\Theta \cos\Theta \tag{15b}$$

$$G_{yx,ij} = G_{xy,ij} \tag{15c}$$

$$G_{yy,ij} = Z_{g,ij}^{TE} \cos^2\Theta + Z_{g,ij}^{TM} \sin^2\Theta \tag{15d}$$

$$Z_{g,ij}^{TE} = Z_{g,ii}^{TE} Z_{t,ii\leftarrow jj}^{TE} \tag{16a}$$

$$Z_{g,ij}^{TM} = Z_{g,ii}^{TM} Z_{t,ii\leftarrow jj}^{TM} \tag{16b}$$

The transfer impedances $Z_{t,ii\leftarrow jj}^{TE}$ and $Z_{t,ii\leftarrow jj}^{TM}$ are calculated with application of the cascade matrix. As known from the transmission line theory, the matrix relates input and output voltages and currents on the section (or several sections) of a transmission line. When the source and destination metal layers are distanced by one dielectric layer (that is $|ii - jj| = 1$), equation (17) applies to the case

$$Z_{t,ii\leftarrow jj}^{TE,TM} = \frac{Y_i^{TE,TM}}{Y_i^{TE,TM} \cosh(\gamma_i t_i) + Y_{L,ii}^{TE,TM} \sinh(\gamma_i t_i)} \tag{17}$$

with $Y_i^{TE,TM}$ being admittances of the dielectric layer between the ii^{th} and jj^{th} metal layers. Admittance $Y_{L,ii}^{TE,TM}$ is the total load admittance connected to the ii^{th} metal layer, when looking from jj^{th} to ii^{th} layer.

Finally, the global impedance matrix [Z] valid for the structure from Fig. 2 (2 dielectric and 3 metal layers) is then

$$[Z] = \begin{bmatrix} G_{00} & G_{01} & G_{02} \\ G_{10} & G_{11} & G_{12} \\ G_{20} & G_{21} & G_{22} \end{bmatrix} \tag{18}$$

which links total currents densities in metal layers 0,1 and 2 and the scattered electric intensities at these layers. Matrix [Z] actually represents the matrix written in the EFIE according to equation (3).

$$\begin{bmatrix} E_{00}^{scat} \\ E_{11}^{scat} \\ E_{22}^{scat} \end{bmatrix} = [Z] \begin{bmatrix} J_{00} \\ J_{11} \\ J_{22} \end{bmatrix} \tag{19}$$

3. Approximation of surface currents

This section discusses use of two different current expansion basis functions. First, non-uniform rooftops and their Fourier transform is given. Second, large domain basis functions defined over quad elements are presented. As a last subsection of this section, solution of the EFIE via the Galerking method (method of moments) is briefly mentioned.

3.1 Roof-top basis functions

Roof-top basis functions are most common basis functions being used for approximation of currents within simple spectral domain codes. Typically, uniform rooftops are being incorporated in order to use FFT for acceleration of double summations (Cwick & Mittra, 1987) or (Wan & Encinar, 1995). If non-uniform rooftops are incorporated, then FFT cannot be used. As an advantage a wider class geometries can analyzed without the restriction of snapping into the uniform grid. This is especially valuable when tuning characteristics of the periodic structure or making optimization of the structures with gradient methods (e.g. Newton one).
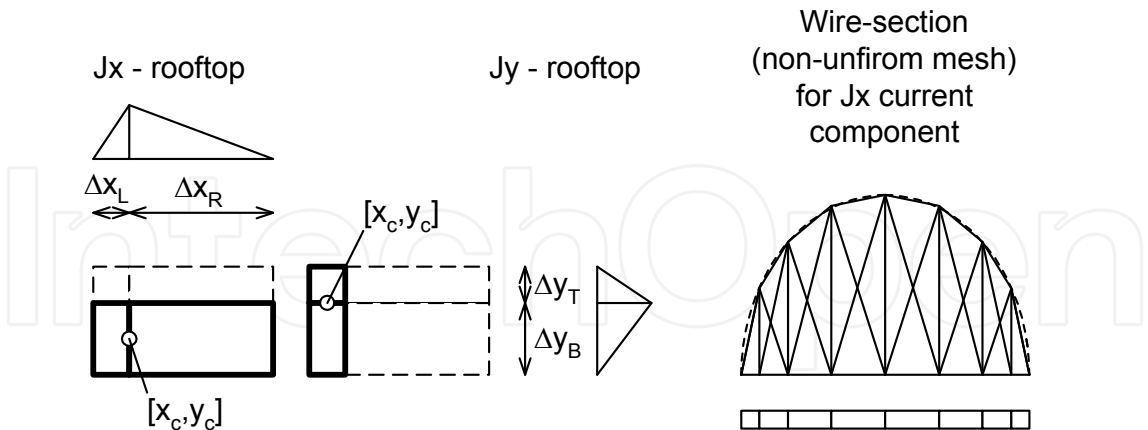

Fig. 3. Non-uniform roof-tops – definition and example of approximation of surface current density

Non-uniform rooftop basis functions are defined in Fig. 3. For example the rooftops being used for approaximation of x-directed currents have lengths of their left and right part denoted as Δx_L and Δx_R. The width of the J_x curent cell is denoted as Δy. The y-directed

rooftops are defined analogically with indexes *L* and *R* being replaced by *B* (bottom) and *T* (top). Fouried transform of the non-uniform rooftops is given in equations (20a) and (20b)

$$F\{B_x(\alpha,\beta)\} = [\Delta_y \sin c(\beta \Delta_y / 2) e^{-j\beta y_c}][\frac{(\Delta x_L + \Delta x_R) - (\Delta x_L e^{-j\alpha \Delta x_R} + \Delta x_R e^{j\alpha \Delta x_L})}{\Delta x_L \Delta x_R \alpha^2} e^{-j\alpha x_c}]$$ (20a)

$$F\{B_y(\alpha,\beta)\} = [\frac{(\Delta y_B + \Delta y_T) - (\Delta y_B e^{-j\beta \Delta y_T} + \Delta y_T e^{j\beta \Delta y_B})}{\Delta y_B \Delta y_T \beta^2} e^{-j\beta y_c}][\Delta_x \sin c(\alpha \Delta_x / 2) e^{-j\alpha x_c}]$$ (20b)

where α and β stand for the space frequency. Symbols x_c and y_c represent x and y co-ordinates of the centre of the J_x or J_y rooftop.

Global approximation of surface currents on conductive patches of the periodic structure, is typically written as

$$J_x(x,y) = \sum_{n_x=1}^{N_x} I_{x,nx} B_{x,nx}(x,y)$$ (21a)

$$J_y(x,y) = \sum_{n_y=1}^{N_y} I_{y,ny} B_{y,ny}(x,y)$$ (21b)

where $B_{x,nx}$ and $B_{y,ny}$ are J_x and J_y rooftop basis functions and $I_{x,nx}$, $I_{y,ny}$ are unknown current expansion coefficients.

Rooftops have generally advantage in easier program implementation and provide good accuracy when analyzing "Manhattan shaped" geometries. Their disadvantage is in the inability to model general or curves patches. Rooftops also provide accurate modelling of amplitude characteristics of FSS. While, the convergence of phase is very slow. These elements are inefficient when analyzing phase shifters in planar reflector antennas (Gona, 2004). In this case, suitable large domain basis functions (e.g. composed from sinusoidal and Tchebyschev functions) must be used.

3.2 Higher-order basis functions defined over quad elements
As a large domain basis functions, historically sinusoidal and cosinusoidal functions were used to represent J_x and J_y current densities over the rectangular patch (Scott, 1989). Alternatively combination of sinusoidal and Tchebyshev functions (Mittra et. al, 1988) may be used. In this case, singular edge currents are well modelled for with low order of expansion functions (typically 2 to 3). During 1990's (Kolundzija, 1998) and (Notaros et al., 2001) extended the use of entire domain basis functions into quadrilaterals (equation 22). These functions satisfy conditions for a local continuity of density and are successfully being used within the modern spatial domain MoM calculations. Their use the spectral domain codes, is less common.
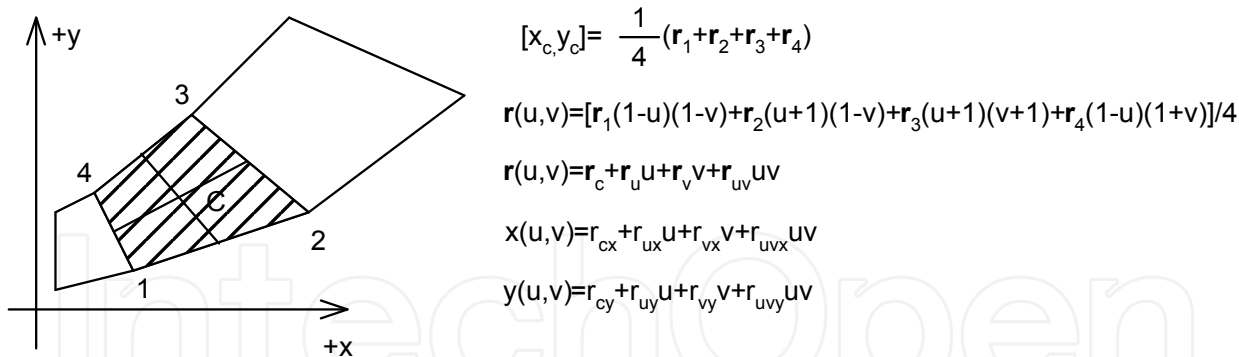
$$[x_c, y_c] = \frac{1}{4}(\mathbf{r}_1 + \mathbf{r}_2 + \mathbf{r}_3 + \mathbf{r}_4)$$

$$\mathbf{r}(u,v) = [\mathbf{r}_1(1-u)(1-v) + \mathbf{r}_2(u+1)(1-v) + \mathbf{r}_3(u+1)(v+1) + \mathbf{r}_4(1-u)(1+v)]/4$$

$$\mathbf{r}(u,v) = \mathbf{r}_c + \mathbf{r}_u u + \mathbf{r}_v v + \mathbf{r}_{uv} uv$$

$$x(u,v) = r_{cx} + r_{ux} u + r_{vx} v + r_{uvx} uv$$

$$y(u,v) = r_{cy} + r_{uy} u + r_{vy} v + r_{uvy} uv$$

Fig. 4. Quadrilateral element – definition

$$\mathbf{J}_u(u,v) = \mathbf{e}_u \left(\sum_{i=0}^{Nu} \sum_{j=0}^{Nv} a_{uij} \begin{cases} 1-u, & i=0 \\ u+1, & i=1 \\ u^i - 1, & i=2,4,...,N_u \\ u^i - u, & i=3,5,....,N_u - 1 \end{cases} \right) v^j \tag{22}$$

where $u,v = <-1;1>$

Large domain basis functions defined according to equation (22) are orthogonal and their Fourier Transform is as following

$$F_x\{J_u(\alpha,\beta)\} = \int_{v=-1}^{v=+1} \int_{u=-1}^{v=+1} J_u(u,v) \cdot e_{ux}(u,v) \cdot e^{-j(\alpha \cdot x(u,v) + \beta \cdot y(u,v))} |J_1(u,v)| \, du\, dv \tag{23a}$$

$$F_y\{J_u(\alpha,\beta)\} = \int_{v=-1}^{v=+1} \int_{u=-1}^{v=+1} J_u(u,v) \cdot e_{uy}(u,v) \cdot e^{-j(\alpha \cdot x(u,v) + \beta \cdot y(u,v))} |J_1(u,v)| \, du\, dv \tag{23b}$$

where $J_1(u,v)$ is Jacobian. The Jacobian can be expressed by equations (23b)

$$J_1(u,v) = c_0 + c_1 u + c_2 v \tag{23c}$$

Constants c_0, c_1, c_2 are found as

$$c_0 = \frac{1}{8}((r_{4x} - r_{2x}) * (r_{1y} - r_{3y}) + (r_{3x} - r_{1x}) * (r_{4y} - r_{2y})) \tag{23d}$$

$$c_1 = \frac{1}{8}((r_{4x} - r_{3x}) * (r_{3y} - r_{1y}) + (r_{1x} - r_{2x}) * (r_{4y} - r_{3y})) \tag{23e}$$

$$c_2 = \frac{1}{8}((r_{4x} - r_{1x}) * (r_{2y} - r_{3y}) + (r_{3x} - r_{2x}) * (r_{4y} - r_{1y})) \tag{23f}$$

where r_{1x}, r_{1y} ; r_{2x}, r_{2y}; r_{3x}, r_{3y}; r_{4x}, r_{4y} are x and y co-ordinates of quadrilateral vertices.
Further details about analytical or semianalytical expressions for the Fourier transform of the J_u current component are beyond the extent of the chapter.

3.3 Solution of current expansion coefficients

Once the suitable current approximation (e.g. rooftops) is selected and the metal patches in all layers are divided into cells, the unknown current expansion coefficients can be determined by the Galerkin method (Scott, 1989) or (Wu, 1995). As a result of the Galerkin testing procedure, a system of linear equations is obtained and unknown current expansion coefficients are solved by the matrix inversion. After solution of the system of equations, current density is evaluated in the spectral domain and scattered electric intensity $\mathbf{E}^{scat}$ in all layers is calculated using equation (4).

Generation of elements a matrix of equations for large number of unknowns is time consuming due to the presence of double summations in the electric field equation. Several methods were introduced during last 20 years. One of them is acceleration of double summations by use of a Poission summation formula or more newly by using hybrid spatial-spectral domain approach (Kipp & Chan, 1994).

3.4 Reflection and transmission coefficients

Prior definition of reflection and transmission coefficients, let's assume that the periodic structure is independently illuminated by a plane wave with parallel (TM) and orthogonal (TE) polarizations (transverse to z). The x and y components of the incident electric intensity are then

$$\mathbf{E}^{inc,TM} = [\cos(\varphi^I) \quad \sin(\varphi^I)] \tag{24a}$$

$$\mathbf{E}^{inc,TE} = [-\sin(\varphi^I) \quad \cos(\varphi^I)] \tag{24b}$$

To compute the reflection and transmission coefficients for a multilayer periodic structure, the electric intensity in the most top (reflected wave E^{refl}) and the electric intensity at the most bottom (transmitted wave E^{trans}) air to dielectric interfaces must be calculated. These intensities are given by equations (25)

$$\mathbf{E}^{refl,TM}_{mm\_\max} = \mathbf{E}^{scat,TM}_{mm\_\max} + \mathbf{E}^{inc,TM}(1+\Gamma^{TM}) \tag{25a}$$

$$\mathbf{E}^{refl,TE}_{mm\_\max} = \mathbf{E}^{scat,TE}_{mm\_\max} + \mathbf{E}^{inc,TE}(1+\Gamma^{TE}) \tag{25b}$$

$$\mathbf{E}^{trans,TM}_{mm=0} = \mathbf{E}^{scat,TM}_{mm=0} + \mathbf{E}^{inc,TM}\mathrm{T}^{TM} \tag{25c}$$

$$\mathbf{E}^{trans,TE}_{mm=0} = \mathbf{E}^{scat,TE}_{mm=0} + \mathbf{E}^{inc,TE}\mathrm{T}^{TE} \tag{25d}$$

where coefficients Γ^{TM}, Γ^{TE} and T^{TM}, T^{TE} are computed according to the procedure described in section 4.

Reflection and transmission coefficients are defined differently by different authors. Most common definition is upon the z-directed potentials (Cwick & Mittra, 1987) or the tangential components of the electric intensity (Wan & Encinar, 1995). In this section, the definition from thesis (Gona, 2004) will be used. The definition is being used in physics related

textbooks and assumes that the electric intensity of the incident and reflected wave are expressed by E_ϑ and E_φ components (Fig. 5).
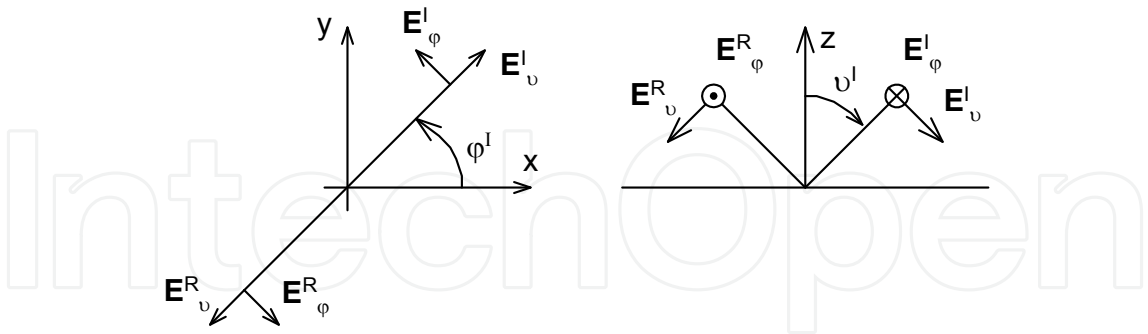

Fig. 5. Definition of reflection coefficients

Reflection coefficients defined by spherical components of the electric intensity are given by the matrix (26).

$$[\rho] = \begin{bmatrix} \rho_{\vartheta\vartheta} & \rho_{\vartheta\varphi} \\ \rho_{\varphi\vartheta} & \rho_{\varphi\varphi} \end{bmatrix} \tag{26}$$

The advantage of the definition is that the cross-polarized reflection coefficients $\rho_{\vartheta\varphi}$ and

$\rho_{\varphi\vartheta}$ are equal.

The definition of reflection coefficients by the tangential components of the electric intensity is more common (Wan & Encinar, 1995) and is given by matrix (27), with cross-polarized terms being different

$$[R] = \begin{bmatrix} R_{TMTM} & R_{TMTE} \\ R_{TETM} & R_{TETE} \end{bmatrix} \tag{27}$$

A relation between definitions (26) and (27) as given in the thesis (Gona, 2004) and is as follows

$$R_{TMTM} = -\rho_{\vartheta\vartheta} \tag{28a}$$

$$R_{TETM} = -\rho_{\varphi\vartheta}\frac{1}{\cos(\vartheta)} \tag{28b}$$

$$R_{TMTE} = -\rho_{\vartheta\varphi}\cos(\vartheta) \tag{28c}$$

$$R_{TETE} = -\rho_{\varphi\varphi} \tag{28d}$$

Once the tangential components of the electric intensity of incident and transmitted wave are evaluated with the aid of equations (25) and (4) then the fundamental mode ((0,0) Floquet mode) reflection transmission coefficients can be obtained by equations (29).

$$\rho_{\vartheta\vartheta} = \frac{1}{\left|E_{TM}^{inc}\right|}\left(-\frac{\cos(\varphi^I)}{\cos(\vartheta^I)}E_{x,mm\_max}^{refl,TM} - \frac{\sin(\varphi^I)}{\cos(\vartheta^I)}E_{y,mm\_max}^{refl,TM}\right) \tag{29a}$$

$$\rho_{\varphi\vartheta} = \frac{1}{\left|E_{TM}^{inc}\right|}(\sin(\varphi^I)E_{x,mm\_\max}^{refl,TM} - \cos(\varphi^I)E_{y,mm\_\max}^{refl,TM}) \tag{29b}$$

where $\left|E_{TM}^{inc}\right| = 1/\cos(\vartheta^I)$ and $E_{x.mm\_\max}^{refl,TM}$, $E_{y,mm\_\max}^{refl,TM}$ are components of the total electric intensity of the reflected wave at the most top layer of the periodic structure (Parallel polarization of the incident plane wave is assumed). According to the example given in Fig. 1, the most top layer is M2. Similarly the coefficients for the orthogonal polarization (TE) are defined

$$\rho_{\vartheta\varphi} = \frac{1}{\left|E_{TE}^{inc}\right|}(-\frac{\cos(\varphi^I)}{\cos(\vartheta^I)}E_{x,mm\_\max}^{refl,TE} - \frac{\sin(\varphi^I)}{\cos(\vartheta^I)}E_{y,mm\_\max}^{refl,TE}) \tag{29c}$$

$$\rho_{\varphi\varphi} = \frac{1}{\left|E_{TE}^{inc}\right|}(\sin(\varphi^I)E_{x,mm\_\max}^{refl,TE} - \cos(\varphi^I)E_{y,mm\_\max}^{refl,TE}) \tag{29d}$$

where $\left|E_{TE}^{inc}\right| = 1$.

Calculation of transmission coefficients is also done with equations (29) but intensities for reflected wave are replaced by intensities from transmitted fields and spherical angles ϑ^I and φ^I are replaced with $-\vartheta^I$ and $\varphi^I + \pi$.

4. Reflection and transmission from a multilayer dielectric structure

The derivation of reflection and transmission coefficients for a multilayer dielectric structure can be found in (Wu, 1995), for example. The derivation makes use of the unitary z-components of the vector potentials $\mathbf{A}_z$ and $\mathbf{F}_z$.

$$\mathbf{A}^{TM} = \mathbf{u}_z A_z = \mathbf{u}_z \psi^{TM} = \mathbf{u}_z e^{j(\alpha_0 x + \beta_0 y)} e^{\gamma_0 z} \tag{30a}$$

$$\mathbf{F}^{TE} = \mathbf{u}_z F_z = \mathbf{u}_z \psi^{TE} = \mathbf{u}_z e^{j(\alpha_0 x + \beta_0 y)} e^{\gamma_0 z} \tag{30b}$$

As known from the electromagnetic theory, the TE and TM polarized plane waves can be derived from the unit $\mathbf{A}_z$ and $\mathbf{F}_z$ potentials by application of a complete set Maxwell equations (that is Maxwell equations with both electric and magnetic currents).

$$\mathbf{E}^{TM} = \frac{1}{j\omega\varepsilon}(\nabla\nabla + k^2 I)\mathbf{A}^{TM} \tag{30a}$$

$$\mathbf{H}^{TM} = \nabla \times \mathbf{A}^{TM} \tag{30b}$$

$$\mathbf{E}^{TE} = -\nabla \times \mathbf{F}^{TE} \tag{30c}$$

$$\mathbf{H}^{TE} = \frac{1}{j\omega\mu}(\nabla\nabla + k^2 I)\mathbf{F}^{TE} \tag{30d}$$

By expressing tangential components E_x and H_y with applications of equations (31) and enforcing continuity of components E_x and H_y at all dielectric and air-to dielectric interfaces, the TM/TE reflection coefficients may be found by solution of matrix equations (32).

$$E_x^{TM} = \frac{1}{j\omega\varepsilon}\frac{\partial^2 \psi^{TM}}{\partial x \partial z} \tag{31a}$$

$$H_y^{TM} = -\frac{\partial \psi^{TM}}{\partial x} \tag{31b}$$

$$E_x^{TE} = -\frac{\partial \psi^{TE}}{\partial y} \tag{31c}$$

$$H_y^{TE} = \frac{1}{j\omega\mu}\frac{\partial^2 \psi^{TE}}{\partial y \partial z} \tag{31d}$$

$$[M^{TM}][x^{TM}] = [b^{TM}] \tag{32a}$$

$$[M^{TE}][x^{TE}] = [b^{TE}] \tag{32b}$$

with $\quad [x^{TM}] = [\Gamma^{TM} \quad C_{11} \quad C_{12} \quad C_{21} \quad C_{22} \quad C_{31} \quad C_{32} \quad T^{TM}]^T$

$$[b^{TM}] = [-\frac{\gamma_0}{\varepsilon_0} \quad 0 \quad 0 \quad 0 \quad -1 \quad 0 \quad 0 \quad 0]^T$$

and $\quad [x^{TE}] = [\Gamma^{TE} \quad C_{11} \quad C_{12} \quad C_{21} \quad C_{22} \quad C_{31} \quad C_{32} \quad T^{TE}]^T$

$$[b^{TE}] = [-1 \quad 0 \quad 0 \quad 0 \quad \gamma_0\frac{\mu_1}{\mu_0} \quad 0 \quad 0 \quad 0]^T,$$

where TM/TE reflection and transmission coefficients are denoted as Γ^{TM}, Γ^{TE} and T^{TM}, T^{TE} respectively. As an example, the matrixes $[M^{TE}]$ and $[M^{TM}]$ for the three-layer dielectric structure (Fig. 6) are given. From the tables 1 and 2 the structure of the $[M^{TE}]$ and $[M^{TM}]$ matrixes for a dielectric structure with general number of layers can be easily derived.
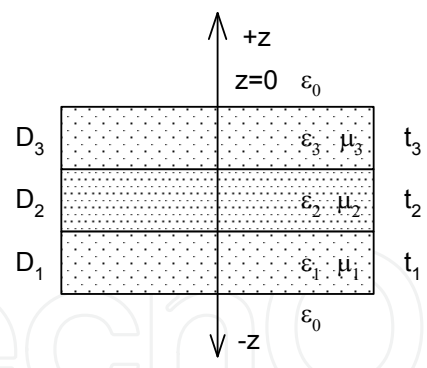
Fig. 6. The 3-layer dielectric structure

$-\gamma_0/\varepsilon_0$	$-\frac{\gamma_1}{\hat\varepsilon_1}\sinh(\gamma_1 t_1)$	$-\frac{\gamma_1}{\hat\varepsilon_1}\cosh(\gamma_1 t_1)$	0	0	0	0	0
0	0	$\gamma_1/\hat\varepsilon_1$	$-\frac{\gamma_2}{\hat\varepsilon_2}\sinh(\gamma_2 t_2)$	$-\frac{\gamma_2}{\hat\varepsilon_2}\cosh(\gamma_2 t_2)$	0	0	0
0	0	0	0	$\gamma_2/\hat\varepsilon_2$	$-\frac{\gamma_3}{\hat\varepsilon_3}\sinh(\gamma_3 t_3)$	$-\frac{\gamma_3}{\hat\varepsilon_3}\cosh(\gamma_3 t_3)$	0
0	0	0	0	0	0	$\gamma_3/\hat\varepsilon_3$	$-\gamma_0/\varepsilon_0$
+1	$-\cosh\gamma_1 t_1)$	$-\sinh(\gamma_1 t_1)$	0	0	0	0	0
0	+1	0	$-\cosh(\gamma_2 t_2)$	$-\sinh(\gamma_2 t_2)$	0	0	0
0	0	0	+1	0	$-\cosh(\gamma_3 t_3)$	$-\sinh(\gamma_3 t_3)$	
0	0	0	0	0	+1	0	-1

Table 1. Matrix M$^{\text{TM}}$(3 layer – dielectric structure)

+1	$-\cosh(\gamma_1 t_1)$	$-\sinh(\gamma_1 t_1)$	0	0	0	0	0
0	+1	0	$-\cosh(\gamma_2 t_2)$	$-\sinh(\gamma_2 t_2)$	0	0	0
0	0	0	+1	0	$-\cosh(\gamma_3 t_3)$	$-\sinh(\gamma_3 t_3)$	0
0	0	0	0	0	+1	0	-1
$\gamma_0\hat\mu_1/\mu_0$	$\gamma_1\sinh(\gamma_1 t_1)$	$\gamma_1\cosh(\gamma_1 t_1)$	0	0	0	0	0
0	0	$\gamma_1\hat\mu_2/\hat\mu_1$	$-\gamma_2\sinh(\gamma_2 t_2)$	$-\gamma_2\cosh(\gamma_2 t_2)$	0	0	0
0	0	0	0	$\gamma_2\hat\mu_3/\hat\mu_2$	$-\gamma_3\sinh(\gamma_3 t_3)$	$-\gamma_3\cosh(\gamma_3 t_3)$	0
0	0	0	0	0	0	$\gamma_3\hat\mu_0/\hat\mu_3$	$-\gamma_0$

Table 2. Matrix M$^{\text{TE}}$ (3 layer – dielectric structure)

5. Numerical examples

This section presents numerical results for reflection and transmission coefficients for periodic structures with different elements (patches). Where available the numerical results are compared with results obtained by other authors. All numerical examples given, were calculated by our in-house periodic MoM code called FSSMQ. The code was written upon the theory presented in the previous sections. At the present, the code allows analysis of periodic structures having up to 4 dielectric and 5 metal layers. At each metal layer, arbitrarily shaped patches may be present. These patches are meshed with uniform or non-uniform rectangular elements depending on the graphical editor being used. As current approximation basis functions, non-uniform rooftops are used. The FSSMQ code is based on a direct approach, that is the global impedance matrix, which relates interactions among all metal layers, is being used for description of interactions among the layers. The program is written in Matlab and can be used for analysis of any planar periodic structures. Its target applications are frequency selective surfaces, composite materials and potentially metamaterials. During solution of a system of linear equations for unknown current expansion coefficients, Matlab's matrix inversion is being used. With this type of solver and speed optimized program architecture, multilayer periodic structures with several hundreds of unknowns may be analyzed within few seconds per frequency (Celeron M, 1.6 GHz). Program allows also interactive postprocessing of currents (surface and vector plots) and total electric intensities at selected layers.

5.1 Jerusalem cross

Jerusalem Cross is one of the oldest elements. It was developed to produce stable reflection coefficients within a large range of angles of incidences (Mittra et al., 1988). The element was analyzed thoroughly by (Cwick & Mittra, 1987) and (Mittra at al., 1988). In this subsection more newer results from (Weile & Michielssen, 2001) are being compared with results from the FSSMQ code.
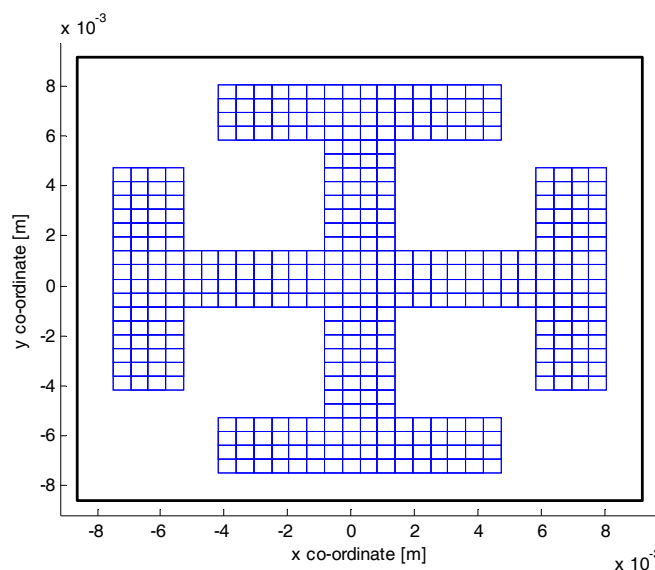
Fig. 7. Jerussalem cross element. Dimensions of the periodic cells $a = b = 17.8$ mm. Discretization 32x32 cells. Relative permittivity 1.0. Maximal number of Floquet harmonics $M = N = 18$

Geometry of the Jerusalem cross which was analyzed is shown in Fig. 7. Dimensions of the periodic cell are $a = b = 17.8$ mm. Periodic cell is divided into 32x32 cells. It is considered that the element resides in free-space and the structure is illuminated by the 40 degree TM polarized wave. Frequency dependence of the TM power reflection coefficient is shown in Fig. 8. It can be seen, that the FSSMQ produces identical results with those given in (Weile & Michielssen, 2001) where resonance arising for oblique incidence is well captured.
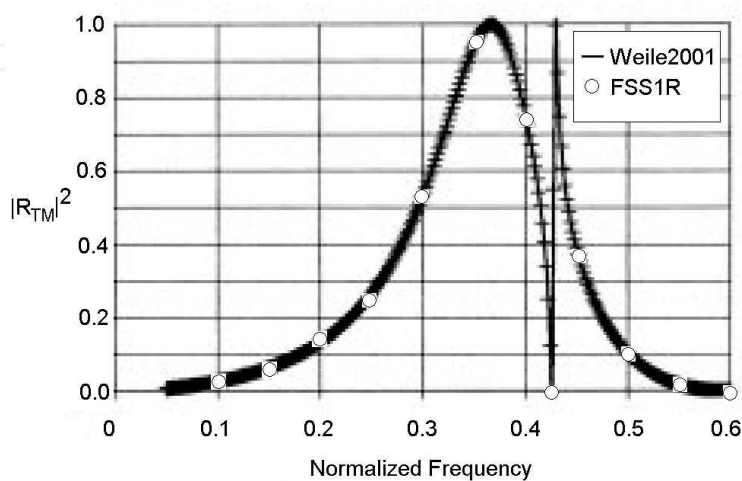
Fig. 8. Power reflection coefficient versus frequency (parallel polarization) , normalization frequency was f_n = c/a = 16.842 GHz, v^l = 40 deg, φ^i = 0 deg

5.2 Cross element

Cross element is often used in practise in design or reflector antennas. However it does not show as superior performance as loop elements (e.g. Fourlegged or square ring element). The element was analyzed by many authors. In this subsection results from (Wan & Encinar, 1995) serve as a reference. In figures 9 and 10, reflection coefficient for a single and a double layer cross element FSS are compared. For the purpose of validation of the FSSMQ code for a single and multilayer case, the same number of Floquet modes as in (Wan, 1995) was selected. In both cases, excellent agreement is observed.
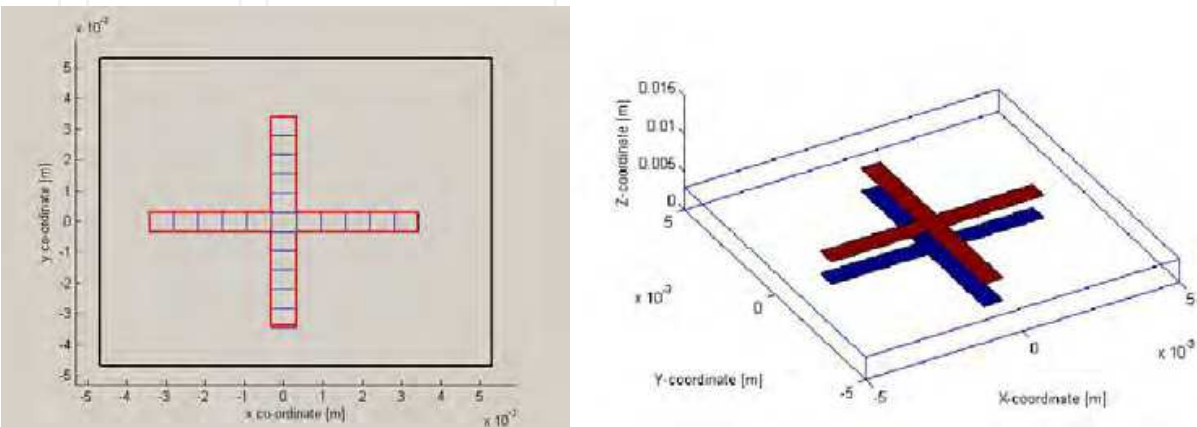
Fig. 9. Left) FSS with cross elements – an elementary cell ($a = b = 10$ mm, 16x16 grid) Right) FSS with two identical cross elements placed in metal layers M_0 and M_1.
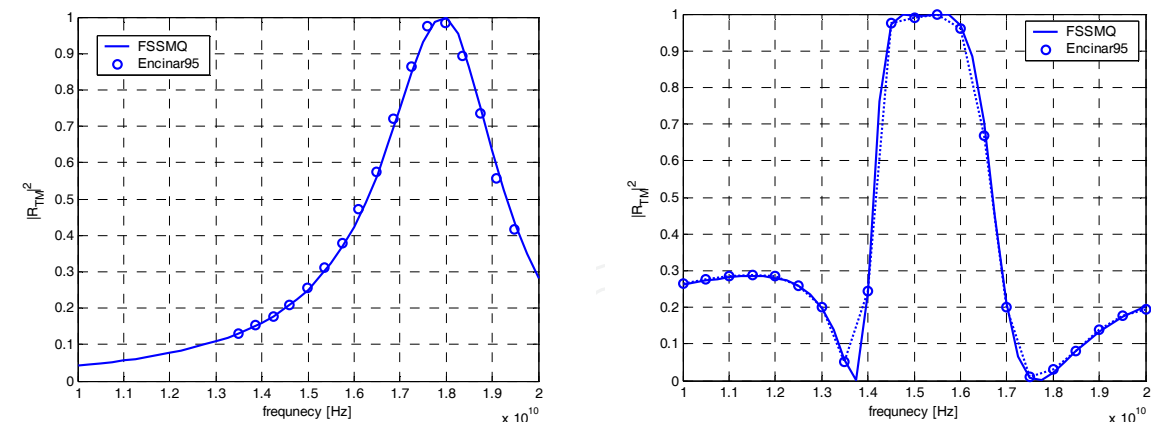
Fig. 10. Power reflection coefficient versus frequency (FSS with cross elements) - comparison of results produced by FSSMQ code and results from (Wan & Encinar, 1995) - cell period $a = b = 10$mm, length of cross dipole $a' = b' = 6.875$ mm, width of cross dipole $w_x = w_y = 0.625$ mm, 16x16 grid). Left) single dielectric and single metal layer, substrate thickness $d = 0.5$ mm, Relative permittivity was 2.0. Right) double cross element, $d = 2.362$ mm, $\varepsilon_r = 2.58$

5.3 Four-legged element

This element is reported as one of the best elements in terms of stability of reflection coefficient with respect to the angle of incidence (Munk, 2000). If properly designed in combination with suitable selection of the relative permittivity of a dielectric substrate, reflection coefficient stays stable well beyond the 45 degrees for all frequencies within the operating band.

Period: a=6.609 mm
Cross length: a_1=6.25mm
Wire width: w=0.171mm
Cross width: c=1.25mm
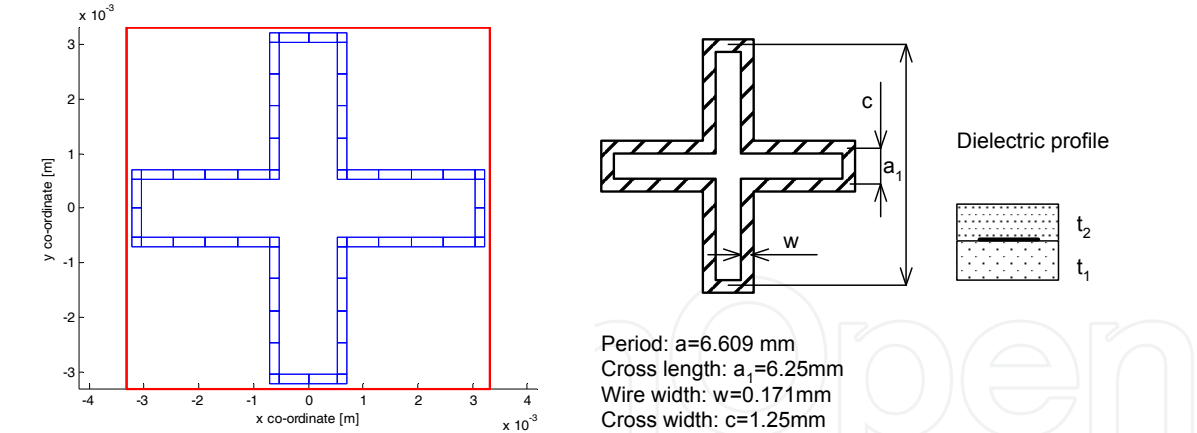
Fig. 11. Left) FSS with four-legged element (Munk, 2000) – non-uniformly meshed with rectangular cells, Right) element dimensions and the dielectric profile ($t_1 = t_2 = 0.508$ mm, $\varepsilon_{r1} = \varepsilon_{r2} = 2.2$)

The geometry of the four-legged element being analyzed is shown in Fig. 11. Its dimensions and properties of the dielectric profile were overtaken from (Munk, 2000). The element was meshed with non-uniform rooftops (Fig. 11, left), contrary to the (Munk, 2000) where large domain basis functions were used. The total number of unknown current expansion coefficients was $N_x + N_y = 26+26 = 52$. The calculation of reflection properties was performed from 1 to 20 GHz, considering an oblique incidence (45 degrees). As seen from Fig. 12, a

very good agreement was obtained between the two approaches. The slight disagreements are attributed to readout errors from the graphs given in (Munk, 2000).
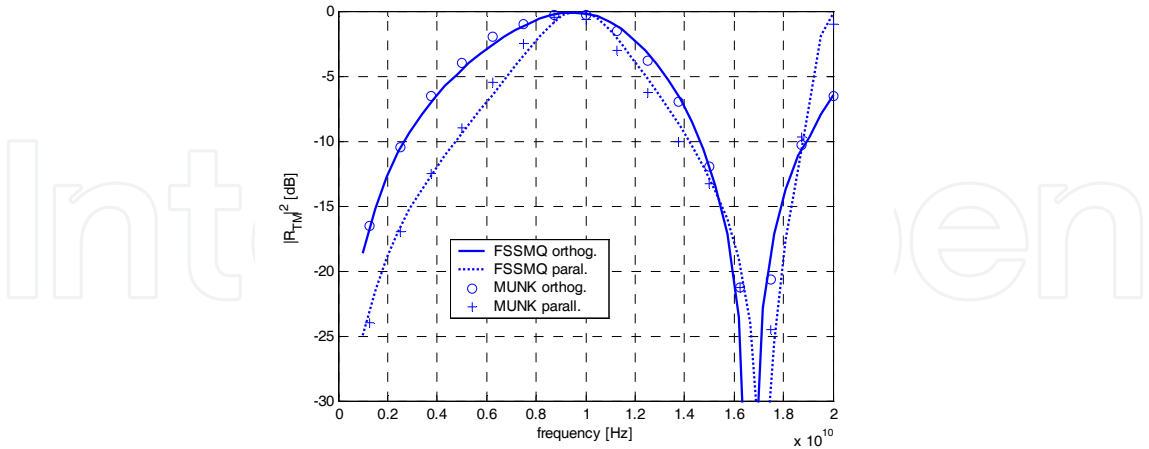

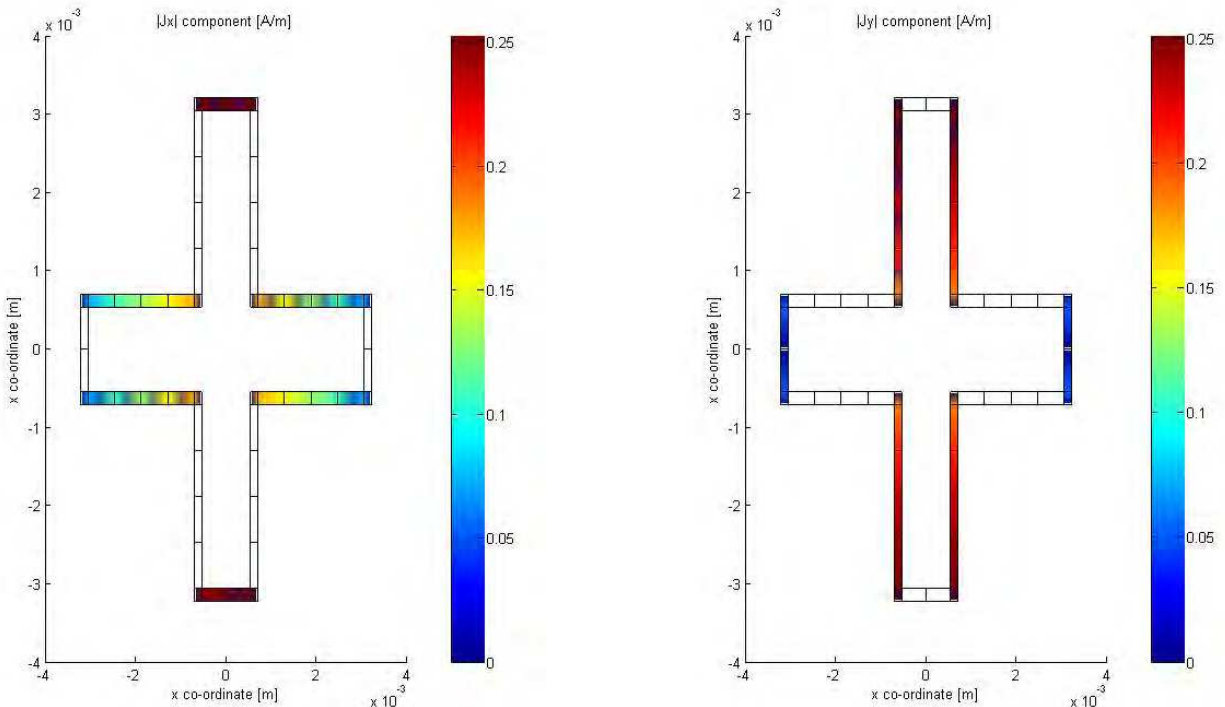Fig. 12a. FSS with four-legged element (TM reflection coefficient versus frequency)

Fig. 12b. FSS with four-legged element (current density at resonance (10 GHz), TM incidence)

5.4 Composite materials – reflectivity study
In this subsection a study of reflection properties of a composite material is presented. The composite material consists from 10 micrometers wide flat fibres (which approximate real rounded ones). Fibres are placed in the y direction with a period of a = 20 micrometers (Fig. 13). Different composite materials have fibres with conductivity ranging from 100 to 10000 S/m. For more details about physical properties of composite materials see for example paper (Jayasree at el, 2008). In this example conductivity γ = 10000 S/m was selected. Three different simulations were performed. First, the composite with a single layer of wires was

analyzed assuming the infinite wire conductivity (Fig. 14). Second, the effect of the finite conductivity was studied. It has been found that shielding effectiveness at 1 GHz was reduced from -85 to -18 dB. Third, three layers of lossy wires distanced 100um apart were analyzed. In this case, the shielding effectiveness improved by 10 dB at 1 GHz. Simulations were performed at frequency range 1-18 GHz. Since at frequencies 1-18 GHz the skin depth was larger than the thickness of the flat wire, the sheet resistance Rs could be approximated as Rs = $1/(\gamma*t)$.

At each metal layer, flat wire was meshed by 50 cells. Number of J_x and J_y current expansion coefficients per one layer was 40 + 50 = 90. For a three layer structure, the global impedance matrix sized 270x270 was assembled. Solution time per one frequency was about 5 seconds (Celeron M, 1.6 GHz).
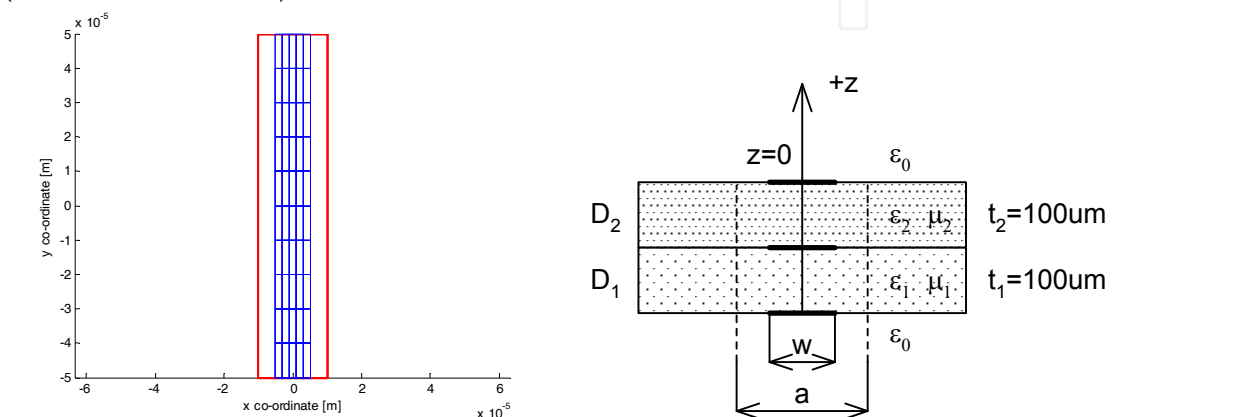
Fig. 13. Composite material with carbon fibres (a = 20um, w = 10um, t = 10um) Left) Meshed fibre, Right) Profile of the composite (t_1 = t_2 = 100 um, ε_{r1} = ε_{r2} = 1)
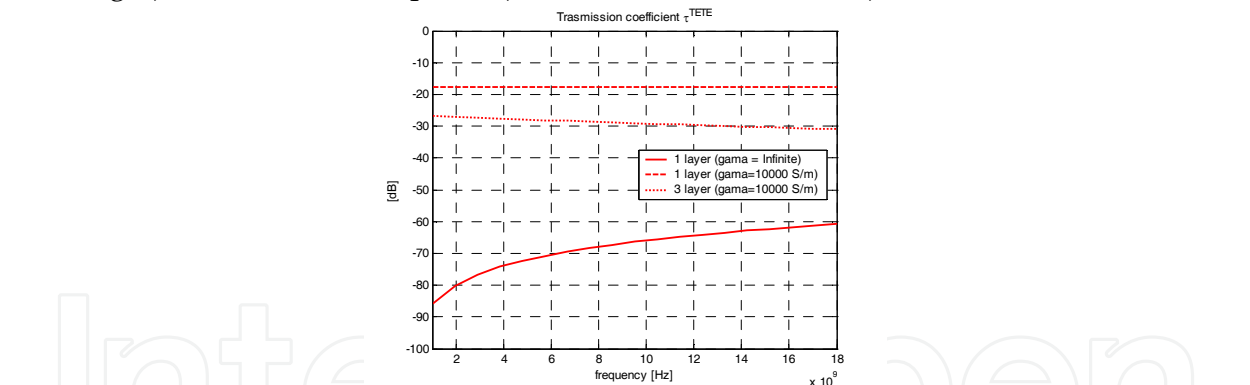

Fig. 14. Transmission coefficient of the composite structure (Number of Floquet harmonics M = N = 18), angle of incidence v^I=0 deg, φ^I = 90 deg (electric intensity parallel with wire).

6. Conclusions

In this chapter, numerical analysis of planar periodic multilayer structures by the spectral domain method was addressed. Compared to other authors, use of non-uniform rooftops and a direct approach of analysis periodic structure with the global impedance matrix, was presented. Briefly, large domain basis functions defined over quadrilateral elements were outlined. Based, on the theory described in previous sections, capabilities of written FSSMQ simulation program were demonstrated on several examples. A very good agreement with results presented by other authors was obtained with the use of the code.

7. References

Itoh, T. (1980). Spectral Domain Immitance Approach for Disperion Chracteristics of Generalized Printed Transmission Lines. *IEEE transactions on Microwave Theory and Techniques,* Vol. 28, No. 7, July 1980, pp. 733-736.

Liu, C., C.; Hessel, A.; Hanfling, J., D., Usoff, J. M. (1985). Plane wave reflection from microstrip patch arrays – Theory and Experiment. *IEEE transactions on Antennas and Propagation,* Vol. 33, No. 4, April 1985, pp. 426-435.

Cwick, T., A.; Mittra, R. (1987). Scattering from a Periodic Array of Free-Standing Arbitrarily Shaped Perfectly Conducting or Resistive Patches. *IEEE transactions on Antennas and Propagation,* Vol. 35, No. 11, Nov 1987, pp. 1226-1234.

Mittra, R.; Chi, H., C.; Cwick, T. (1988). Techniques for Analyzing Frequnecy Selective Surfaces – A Review. *IEEE Proceedings,* Vol. 76, No. 2, Dec 1988, pp. 1593-1615.

Scott, G. (1989). *Spectral domain method in electromagnetics,* Artech House, New York.

Wu, T., K. (1995). *Frequency selective Surfaces and Grid Arrays,* John Wiley & Sons, ISBN 0-471-31189-8, New York.

Kipp, R., A.; Chan, C., H. (1994). A numerically Efficient Technique for the Method of Moments Solution for Planar Periodic Structures in Layered Media. *IEEE Transactions on Microwave Theory and Technique,* Vol. 42, No. 4, Apr 1994, pp. 635-642.

Wan, C.; Encinar, J., A. (1995). Efficient Computation of Generalized Scattering Matrix For Analyzing Multilayered Periodic Structures. *IEEE Transactions on Antennas and Propagation,* Vol. 43, No. 11, Dec 1995, pp. 1233-1242.

Kolundzija, B. (1998). On the Locally Continuous Formulation of Surface Doublets. *IEEE Transactions on Antennas and Propagation,* Vol. 46, No. 12, Dec 1998, pp. 1879-1883.

Gona, S.; Raida, Z. (1999). Hybrid FE/SD MoM analysis of frequency selective surfaces with arbitrarily shaped elements. *In proceedings of the international conference on electronics in advanced applications (ICEAA 99), Sept* 13-17, 1999, Torino, Italy.

Munk, B., A. (2000). *Frequency selective Surfaces – Theory and Design,* John Wiley & Sons, ISBN 0-471-37047-9, New York.

Notaros, M., B.; Popovic, B., D.; Weem, J., P.; Brown, R., A.; Popovic, Z. Efficient Large-Domain MoM Solutions to Electrically Large Practical EM Problems. *IEEE Transactions on Microwave Theory and Techniques,* Vol. 49, No. 1, Jan 2001, pp. 151-159.

Weile, D., S.; Michielssen, E. (2001); Galivan, K. Reduced-Order Modeling of Multiscreen Frequency-Selective Surfaces Using Krylov-Based Rational Interpolationn. *IEEE Transactions on Antennas and Propagation,* Vol. 49, No. 5, May 2001, pp. 801-813.

Gona, S. (2004). *Analysis and design of planar reflector antennas,* Ph.D Thesis. Brno University of Technology, Brno.

Gona, S.; Kresalek, V. (2008). Development of a Versatile Planar Periodic Structure Simulator in MATLAB. *In proceedings of the international conference on microwave techniques (COMITE 2008),* Apr23-24 2008, pp. 335-338. ISBN 978-1-4244-2137-4. Prague.

Jayasree, P., V., Y.; Baba, V., S., S., N.; Rao, B., P. (2008). Shielding Effectiveness of Laminated Shields. *Radioengineering magazine,* Vol. 17, No. 4, Dec 2008.
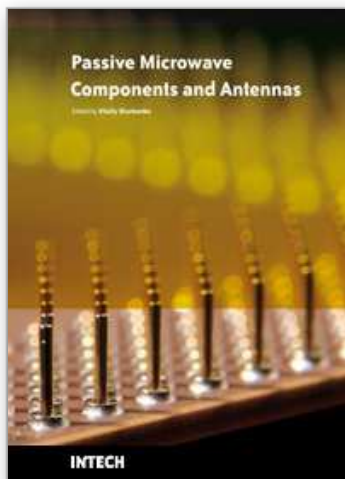
Passive Microwave Components and Antennas

Edited by Vitaliy Zhurbenko

Modelling and computations in electromagnetics is a quite fast-growing research area. The recent interest in this field is caused by the increased demand for designing complex microwave components, modeling electromagnetic materials, and rapid increase in computational power for calculation of complex electromagnetic problems. The first part of this book is devoted to the advances in the analysis techniques such as method of moments, finite-difference time- domain method, boundary perturbation theory, Fourier analysis, mode-matching method, and analysis based on circuit theory. These techniques are considered with regard to several challenging technological applications such as those related to electrically large devices, scattering in layered structures, photonic crystals, and artificial materials. The second part of the book deals with waveguides, transmission lines and transitions. This includes microstrip lines (MSL), slot waveguides, substrate integrated waveguides (SIW), vertical transmission lines in multilayer media as well as MSL to SIW and MSL to slot line transitions.

How to reference

In order to correctly reference this scholarly work, feel free to copy and paste the following:

INTECH

open science | open minds